

Electrostatic waves driven by electron beam in lunar wake plasma

T. Sreeraj,^{a)} S. V. Singh,^{b)} and G. S. Lakhina^{c)}

Indian Institute of Geomagnetism, New Panvel (West), Navi Mumbai, Maharashtra 410218, India

(Received 3 April 2018; accepted 25 April 2018; published online 15 May 2018)

A linear analysis of electrostatic waves propagating parallel to the ambient field in a four component homogeneous, collisionless, magnetised plasma comprising fluid protons, fluid He⁺⁺, electron beam, and suprathermal electrons following kappa distribution is presented. In the absence of electron beam streaming, numerical analysis of the dispersion relation shows six modes: two electron acoustic modes (modes 1 and 6), two fast ion acoustic modes (modes 2 and 5), and two slow ion acoustic modes (modes 3 and 4). The modes 1, 2 and 3 and modes 4, 5, and 6 have positive and negative phase speeds, respectively. With an increase in electron beam speed, the mode 6 gets affected the most and the phase speed turns positive from negative. The mode 6 thus starts to merge with modes 2 and 3 and generates the electron beam driven fast and slow ion acoustic waves unstable with a finite growth. The electron beam driven slow ion-acoustic waves occur at lower wavenumbers, whereas fast ion-acoustic waves occur at a large value of wavenumbers. The effect of various other parameters has also been studied. We have applied this analysis to the electrostatic waves observed in lunar wake during the first flyby of the ARTEMIS mission. The analysis shows that the low (high) frequency waves observed in the lunar wake could be the electron beam driven slow (fast) ion-acoustic modes. *Published by AIP Publishing.* <https://doi.org/10.1063/1.5032141>

I. INTRODUCTION

Interaction of solar wind with moon has been studied in great detail, with the advent of new space technologies. The moon acts as an obstacle that intercepts and absorbs much of the streaming solar wind and energetic particles on its sunlit surface, creating a downstream plasma-void cavity left behind it for several lunar radii. This region is known as the lunar wake region. Several studies had been undertaken to understand various processes in this region.^{1,2} The WIND satellite, which was launched on November 1, 1994 significantly increased the understanding of lunar wake.³ Initially, it was thought that beyond 4 lunar radii, evidence of the lunar wake will not be observable;⁴ however, WIND spacecraft observations^{5,6} have shown the presence of the lunar wake at a distance of $\sim 6.8 R_L$, where R_L stands for the lunar radius. Simulation studies by Farrell *et al.*⁷ have shown the presence of counter streaming ion beams and rarefaction wave emanating outward from the wake which were consistent with the satellite observations.⁶ The existence of ion and electron rarefaction waves and an increase in the temperature of the electrons were observed by Birch and Chapman⁸ in their simulations. Recently, Xie *et al.*⁹ studied the interaction between the Moon and the solar wind under three different interplanetary magnetic field conditions using three-dimensional MHD simulation. They showed that an acceleration region may appear in the void when the plasma temperature is enhanced. Also, they reported that fast magnetosonic waves propagate away from the limb as the plasma moves in the wake. In recent years, wave phenomena in the vicinity of the Moon have gained considerable importance. Popel *et al.*¹⁰

showed that the relative motion of the solar wind with respect to the photoelectrons over the lunar surface can lead to the excitation of high-frequency oscillations such as Langmuir and electromagnetic waves on the lunar dayside and the dust-acoustic waves in the vicinity of the lunar terminator. Popel *et al.*¹¹ have shown the possibility of the existence of a dusty plasma sheath-like structure with large electric fields of the order of 300 V/m in the lunar terminator region. Recently, Popel and Morozova¹² have shown that interaction of the Earth's magnetotail with the dusty plasma near the lunar surface can lead to the excitation of ion-acoustic and dust-acoustic waves. Because of the relatively long growth time of these instabilities, ion-acoustic as well as dust-acoustic plasma turbulence may develop. Planned future missions such as Luna-25 and Luna-27 lunar modules will have the potential to detect and unravel the manifestations of the low and high frequency wave motions near the lunar surface.¹²

The electrostatic and electromagnetic plasma waves such as ion-acoustic, Langmuir, and whistler waves have been observed in the wake region which is a natural laboratory for observation of these waves.^{13–16} The simulation studies have predicted a variety of instabilities, e.g., two-stream electron instabilities, bump-on-tail instabilities, ion acoustic-like beam instabilities, flute instabilities, and low-frequency electromagnetic waves near local proton cyclotron frequency.^{7,8,17–19}

A detailed analysis of the electrostatic waves observed by the ARTEMIS P1 spacecraft on the outbound side of the flyby has been presented by Tao *et al.*²⁰ They also performed 1-D Vlasov simulation of a four-component plasma comprising protons, ions, an electron beam, and suprathermal (κ -distribution) electrons. They were able to explain the physical properties of the observed electrostatic waves in the frequency range of $(0.1–0.4)f_{pe}$; f_{pe} is the electron plasma frequency and concluded that the observed waves were most likely the electron beam

^{a)}Electronic mail: sreerajt90@gmail.com

^{b)}Electronic mail: satyavir@iigs.iigm.res.in

^{c)}Electronic mail: gslakhina@gmail.com

mode. However, observations below $0.1f_{pe}$ did not find any explanation. Recently, Rubia *et al.*²¹ performed a nonlinear analysis of 4 component plasma comprising hot protons, hot heavier ions (α -particles, He^{++}), electron beam, and suprathermal electrons following kappa distribution. They have proposed an alternate generation mechanism for the electrostatic waves in terms of slow and fast ion-acoustic and electron-acoustic solitons. They could successfully explain the observed low and high frequency waves in the lunar wake.

It is important to mention here that there have been a number of nonlinear studies on the slow and fast ion-acoustic solitons and double layers^{21–28} but to the authors' knowledge, none in the linear regime. Therefore, we undertake a linear dispersion analysis of lunar wake plasma with the model as taken up by Rubia *et al.*²¹ The purpose of this study is to understand how electron beam affects the various modes, e.g., low-frequency (slow and fast ion-acoustic) and high-frequency (electron-acoustic) modes. The paper is organized as follows: In Sec. II, a linear dispersion relation of the model is derived. In Sec. III, numerical results are presented and in Sec. IV, discussions and conclusions are given.

II. THEORETICAL MODEL

The lunar wake plasma is modeled by a homogeneous, collisionless, and magnetized four-component plasma comprising fluid protons (N_{p0} , T_p), doubly charged fluid alpha particles, He^{++} (N_{i0} , T_i), electron beam streaming along ambient magnetic field (N_{b0} , T_b , U_b), and suprathermal electrons (N_{e0} , T_e). Here, N_{s0} and T_s represent the equilibrium values of the density and temperature of the species s , and $s = p, i, b,$ and e for protons, alpha particles, electron beam, and suprathermal electrons, respectively, U_b is the drift speed of the beam electrons. We consider the electrostatic waves propagating parallel to the ambient magnetic field. In such a case, the presence of magnetic field does not affect the propagation properties of the waves. The fluid equations which govern the propagation characteristic of plasma waves are

$$\frac{\partial n_s}{\partial t} + \nabla \cdot (n_s \mathbf{v}_s) = 0, \quad (1)$$

$$m_s n_s \left[\frac{\partial \mathbf{v}_s}{\partial t} + (\mathbf{v}_s \cdot \nabla) \mathbf{v}_s \right] = q_s n_s (-\nabla \phi) - \nabla P_s, \quad (2)$$

$$\nabla^2 \phi = -4\pi e (n_p + n_i z_i - n_e), \quad (3)$$

where m_s , \mathbf{v}_s , P_s , z_i , and q_s represent, respectively, mass, velocity, pressure, atomic number, and charge of the individual species. The pressure term in this case becomes $\nabla P_s = \gamma_s T_s \nabla n_s$, where $\gamma_s = 3$ is the ratio of specific heats for specie "s."

The suprathermal electrons are assumed to have κ distribution which is given by²⁹

$$f_\kappa(v) = \frac{N_{e0}}{\pi^{\frac{3}{2}} \theta^3} \frac{\Gamma(\kappa + 1)}{\kappa^{\frac{3}{2}} \Gamma\left(\kappa - \frac{1}{2}\right)} \left(1 + \frac{v^2}{\kappa \theta^2}\right)^{-(\kappa+1)}, \quad (4)$$

where κ is the superthermality index; Γ is the gamma function; $\theta = \left[\frac{2\kappa-3}{\kappa}\right]^{\frac{1}{2}} \left(\frac{T_e}{m_e}\right)^{\frac{1}{2}}$ is the effective thermal speed and N_{e0} is the equilibrium density of suprathermal electrons. It has to be emphasized that in order to have meaningful value for the thermal speed of suprathermal electrons, we need to have $\kappa > \frac{3}{2}$.

The number density of electrons in the presence of electrostatic waves having potential ϕ can be obtained by replacing v^2/θ^2 by $v^2/\theta^2 - 2e\phi/m_e\theta^2$ in Eq. (4) and by integrating it over velocity space^{30–32}

$$n_{e1} = N_{e0} \left[1 - \frac{e\phi}{T_e \left(\kappa - \frac{3}{2}\right)} \right]^{\frac{1}{2}-\kappa}. \quad (5)$$

Linearization and simplification of Eqs. (1) to (3) and (5) yield the following general dispersion relation:

$$1 + \frac{\omega_{pe}^2}{k^2 v_{te}^2} \frac{2\kappa - 1}{2\kappa - 3} = \frac{\omega_{pb}^2}{(\omega - kU_b)^2 - 3k^2 v_{te}^2} + \frac{\omega_{pp}^2}{\omega^2 - 3k^2 v_{tp}^2} + \frac{z_i^2 \omega_{pi}^2}{\omega^2 - 3k^2 v_{ti}^2}. \quad (6)$$

Here, $\omega_{ps} = \sqrt{4\pi N_{0s} e^2 / m_s}$ is the plasma frequency of s th species. This is similar to the expression which has been derived by Devanandhan *et al.*,³⁰ where they have unmagnetized plasma having cold electrons and ions, superthermal hot electrons, and an electron beam, but have studied electron acoustic waves.

III. NUMERICAL RESULTS

In this section, we carry out the numerical computations of the general dispersion relation (6) for the lunar wake plasma parameters. The relevant lunar wake and solar wind plasma parameters for the computations are taken from the study by Tao *et al.*²⁰ and Mangeney *et al.*³³ In order to facilitate the numerical analysis of Eq. (6), the following normalizations are used: frequencies are normalized by effective proton plasma frequency, $\omega_{p0} = \sqrt{4\pi N_0 e^2 / m_p}$ where N_0 is the total equilibrium electron number density given by the expression $N_0 = N_{p0} + z_i N_{i0} = N_{e0} + N_{b0}$, wave number k with effective hot electron Debye length $\lambda_{de} = \sqrt{T_e / 4\pi N_0 e^2}$ and the velocities are normalized with ion acoustic velocity C_s given by the expression $C_s = \sqrt{T_e / m_p}$.

Before we proceed further, it is important to describe how the different electrostatic wave modes are identified. Initially, we put electron beam density to zero ($N_{b0} = 0$), we obtain four modes: two with positive phase speed and two with negative phase speed which are symmetrical. The modes with lower phase speeds are identified as slow ion-acoustic modes, whereas those with higher phase speeds as fast ion-acoustic modes.²² Then, we introduce electron beam but neglect the streaming, now additional two modes (with positive and negative phase speeds) with highest phase speeds appear along with slow and fast ion-acoustic modes. The modes with the highest phase speed are identified as electron-acoustic modes.²¹ Thus, the six modes are identified

as electron acoustic with positive phase speed (mode 1, dashed-dotted curve, pink color) and negative phase speed (mode 6, solid curve, black color), fast ion-acoustic mode with positive phase speed (mode 2, short dashed curve, blue color) and negative phase speed (mode 5, long dashed curve, green color), and slow ion-acoustic mode with positive phase speed (mode 3, dashed-dotted-dotted-dotted curve, red color) and negative phase speed (mode 4, medium dashed curve, magenta color). In Fig. 1 and subsequent figures, these are clearly identified. Also, it must be noted that real frequencies and growth rates (wherever applicable) are plotted in upper and lower panels, respectively. In Sec. III A, we present the effect of electron beam velocity on the instability.

A. Effect of electron beam velocity

In Fig. 1, the characteristics of dispersion relation (6) are studied by taking into account the effect of electron beam variation. Figure 1(a) shows the plot of ω_r/ω_{p0} versus $k\lambda_{de}$ for $U_b/C_s = 0$. The other fixed plasma parameters^{20,25,33} are $n_b/N_0 = 0.01$, $n_i/N_0 = 0.05$, $\kappa = 6$, $T_b/T_e = 0.0025$, $T_p/T_e = 0.2$, and $T_i/T_e = 0.4$. With $U_b/C_s = 0$, six real roots are obtained, three positive and three negative which are shown by six curves in Fig. 1(a). These six modes are identified as: two electron acoustic modes (modes 1 and 6), two fast ion acoustic modes (modes 2 and 5), and two slow ion acoustic modes (modes 3 and 4). The modes 1, 2, and 3 have positive

phase speeds, whereas modes 4, 5, and 6 have negative phase speeds. All these curves are perfectly symmetrical about the x-axis.

In Figs. 1(b) and 1(c), the electron beam velocity is increased to $U_b/C_s = 2$ and $U_b/C_s = 4$, respectively. It can be seen that the frequency of the modes 1 and 6 is affected the most as compared to that of modes 2, 3, 4, and 5. The frequency of the modes 1 and 6 increases drastically for a fixed value of $k\lambda_{de}$. In fact, phase speed of mode 6 turns positive from negative when U_b/C_s is increased from 0 to 4, whereas electron beam speed has an insignificant effect on other modes, i.e., modes 2 to 5.

When the normalized electron beam velocity is increased further to a value of 4.3 [Fig. 1(d)], the dispersion curves for modes 1 and 6 change drastically. Here, it can be seen that mode 6 (electron acoustic mode) and mode 3 (slow ion acoustic mode) merge in the range $k\lambda_{de} \approx 6.4\text{--}8.6$, i.e., in this $k\lambda_{de}$ range the phase speeds of both the modes become the same and modes merge together and become unstable with a finite growth rate as can be seen in the lower panel of Fig. 1(d). This is an electron beam driven slow ion-acoustic mode. The maximum value of the growth rate is $\omega_i/\omega_{p0} \approx 0.041$ at $k\lambda_{de} = 7.45$ with corresponding real frequency, $\omega_r/\omega_{p0} \approx 4.1$.

For electron beam speed $U_b/C_s = 4.5$ the merging of modes occurs at two places: first at $k\lambda_{de} = 1.87\text{--}2.88$ where mode 6 merges with mode 3 (this is electron beam driven slow ion-acoustic mode) and then again mode 6 merges with

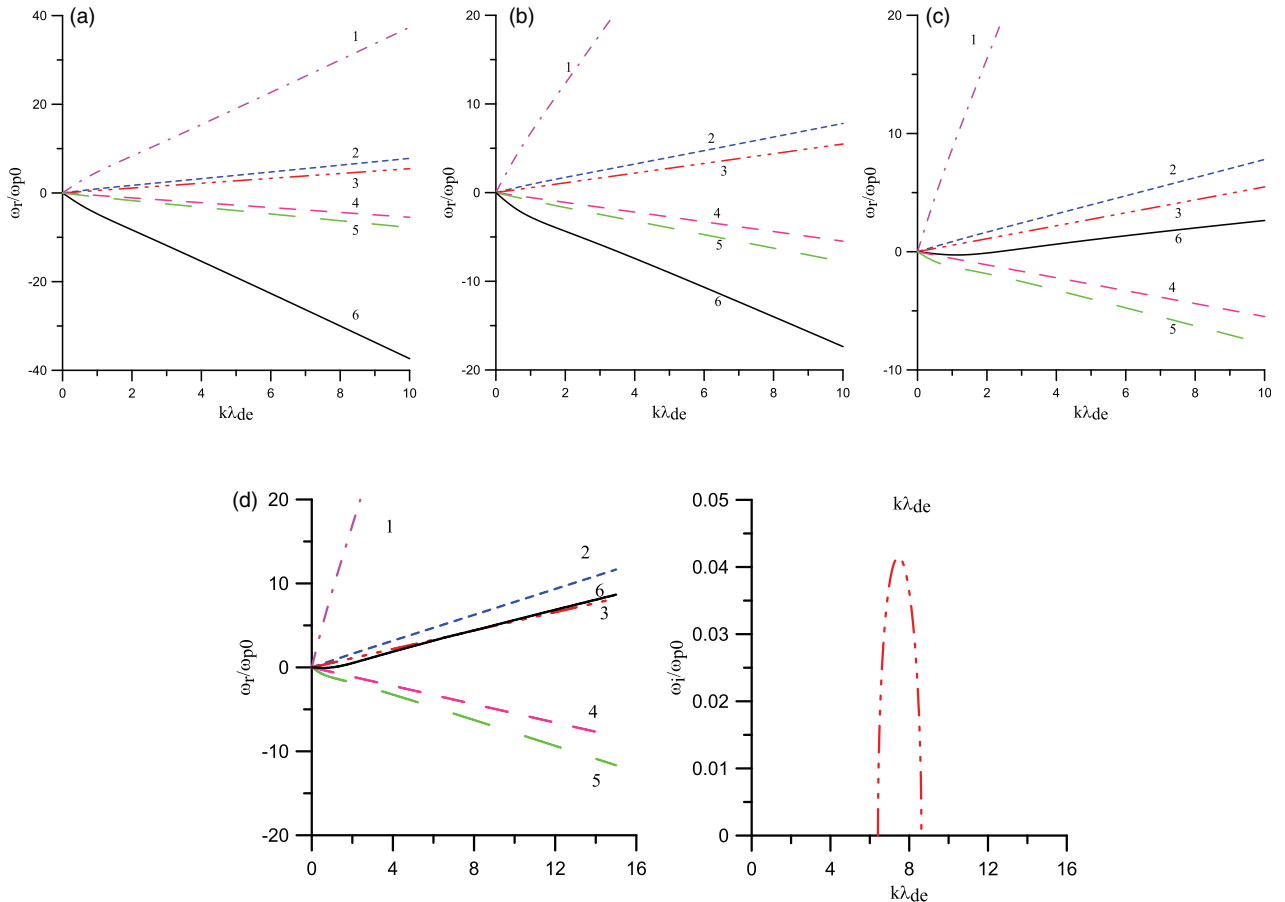


FIG. 1. Plot of real frequency, ω_r/ω_{p0} and growth rate, ω_i/ω_{p0} versus $k\lambda_{de}$ for the fixed parameters $n_b/N_0 = 0.01$, $n_i/N_0 = 0.05$, $\kappa = 6$, $T_b/T_e = 0.0025$, $T_p/T_e = 0.2$, $T_i/T_e = 0.4$, and various values of normalized electron beam speed, U_b/C_s . (a) $U_b/C_s = 0.0$, (b) $U_b/C_s = 2$, (c) $U_b/C_s = 4$, and (d) $U_b/C_s = 4.3$.

mode 2 at $k\lambda_{de} = 6.83\text{--}19.98$ (this is an electron beam driven fast ion-acoustic mode) [see Fig. 2(a)]. First merging happens in a smaller range of wavenumbers, whereas second merging occurs over a broad range and at larger values of wavenumbers. In the first case i.e., the electron beam driven slow ion-acoustic mode, the maximum value of $\omega_i/\omega_{p0} \approx 0.09$ at $k\lambda_{de} = 2.38$ with corresponding real frequency, $\omega_r/\omega_{p0} \approx 1.31$ and for the second case, i.e., electron beam driven fast ion-acoustic mode, $\omega_i/\omega_{p0} \approx 0.088$ at $k\lambda_{de} = 11.78$ with $\omega_r/\omega_{p0} \approx 9.12$. It is seen that the maximum growth rates in the two cases are comparable. Thereafter, when the value of U_B/C_s is increased to 4.6 [Fig. 2(b)], the merging of modes again occurs at two places, first at the $k\lambda_{de} \approx 1.18\text{--}2.02$ and second 2.06 to 6.79. The former merging represents the electron

beam driven slow ion-acoustic mode, whereas the latter represents the electron beam driven fast ion-acoustic mode. From Fig. 2(b), it is also clear that the maximum value of ω_i/ω_{p0} for the electron beam driven slow ion-acoustic mode is ≈ 0.11 at $k\lambda_{de} = 1.69$ with $\omega_r/\omega_{p0} \approx 0.94$ and for the electron beam driven fast ion-acoustic mode it is 0.24 at $k\lambda_{de} \approx 4$ with $\omega_r/\omega_{p0} = 3.11$. Interestingly, the peak growth rate for the electron beam driven fast ion-acoustic modes is nearly twice than that of the slow ion-acoustic mode. A similar trend continues as U_B/C_s increased to 5.4, fast ion-acoustic continues to grow with a larger growth rate and slow ion-acoustic wave growth diminishes.

The dispersion plot for $U_b/C_s = 5.5$ is plotted in Fig. 2(c). It is clear from the figure that there is no interaction

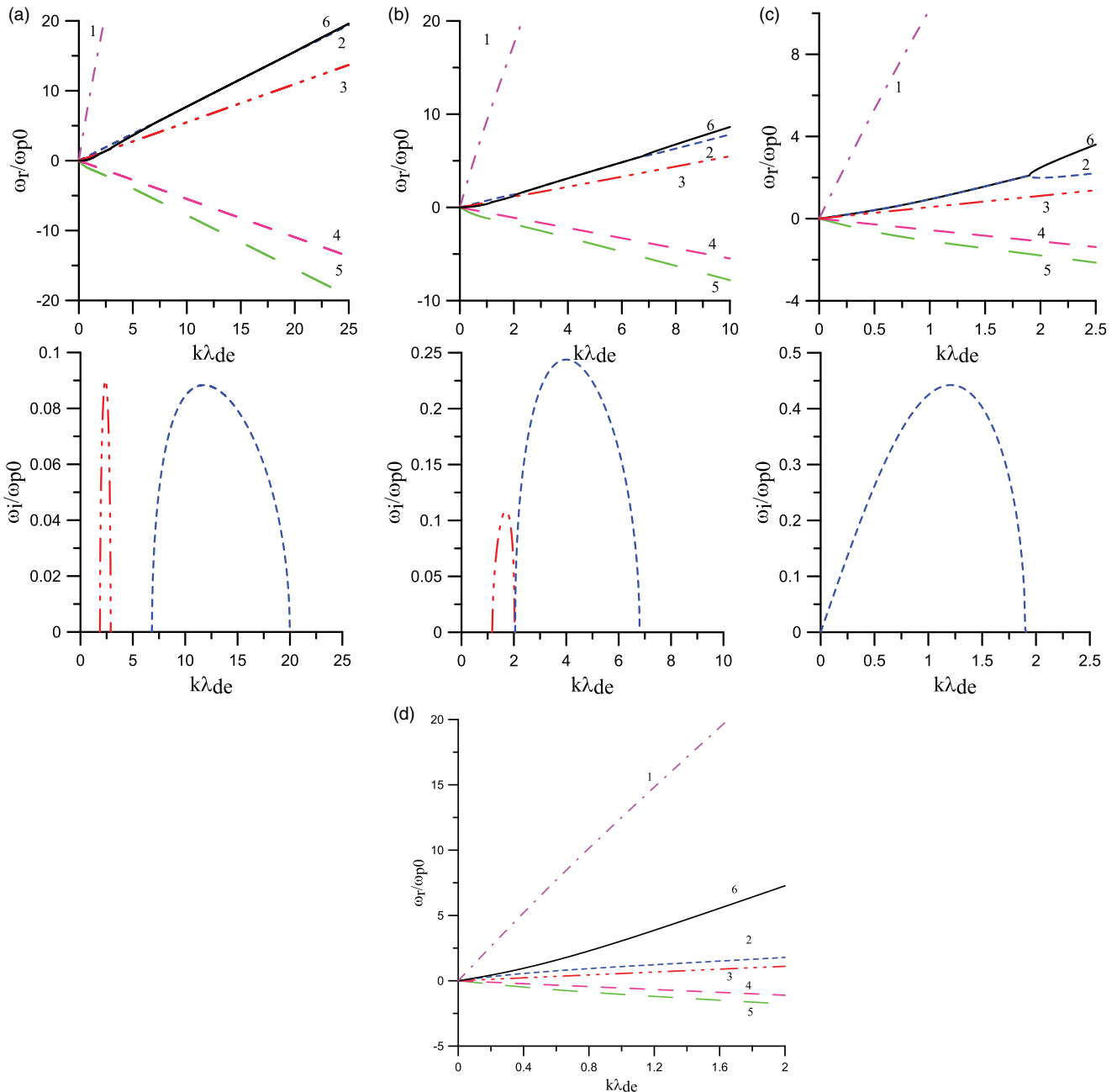


FIG. 2. Plot of real frequency ω_r/ω_{p0} and growth rate, ω_i/ω_{p0} versus $k\lambda_{de}$. All other plasma parameters are the same as those in Fig. 1. (a) $U_b/C_s = 4.5$, (b) $U_b/C_s = 4.6$, (c) $U_b/C_s = 5.5$, and (d) $U_b/C_s = 7.8$.

between the electron beam (mode 6) and slow ion-acoustic (mode 3) and hence, the slow ion-acoustic mode become stable. In this case, only the electron beam driven fast ion-acoustic mode is unstable. The maximum value of the growth rate ω_i/ω_{p0} in this case is 0.44 at $k\lambda_{de}=1.21$ with corresponding real frequency, $\omega_r/\omega_{p0}=1.2$. The $k\lambda_{de}$ range in which the electron beam driven fast ion-acoustic mode is unstable is $k\lambda_{de}\approx 0-1.9$. The unstable region shifts towards a lower wavenumber region with an increase in U_b/C_s . The growth rate of fast ion-acoustic waves starts to decrease at $U_b/C_s > 5.5$ and continues to decrease until $U_b/C_s = 7.7$. The unstable region for these waves disappears at $U_b/C_s = 7.8$ and beyond as is clear from Fig. 2(d) which shows no interaction between the electron beam mode and other modes as all modes remain distinct. In Sec. III B, we study the effect of density of electron beam on the dispersion of the waves.

B. Effect of electron beam density

Here, we study the effect of variation of number density of beam electrons on the dispersion characteristics of the various wave modes. The fixed plasma parameters for these variations are $n_b/N_0=0.05$, $\kappa=6$, $T_b/T_e=0.0025$, $T_p/T_e=0.2$, $T_i/T_e=0.4$, and $U_b/C_s=5$. It can be seen from Fig. 3(a) that at $n_b/N_0=0.1$, both the electron beam driven slow ion-acoustic mode (merging of mode 6 and 3) and fast ion-acoustic mode (merging of modes 6 and 2) are unstable with maximum growth rates of $\omega_i/\omega_{p0}\approx 0.19$ and 0.52, respectively. As we increase the value of n_b/N_0 to 0.2 [Fig. 3(b)] and 0.3 [Fig. 3(c)], the unstable regions for both the modes

shift towards a higher $k\lambda_{de}$ range. However, the growth rates marginally decrease for the electron beam driven slow ion-acoustic mode and increase for the electron beam driven fast ion-acoustic mode. Furthermore, the separation between electron beam driven slow and fast ion-acoustic modes increases with an increase in the value of electron beam density.

C. Variation of density of helium ions

In this subsection, the effect of variation of number density of Helium ions is studied on the dispersion characteristic of the waves. The fixed plasma parameters for Fig. 4 are $n_b/N_0=0.01$, $\kappa=6$, $T_b/T_e=0.0025$, $T_p/T_e=0.2$, $T_i/T_e=0.4$, and $U_b/C_s=5$. We have plotted real frequency (upper panel) and growth rates (lower panels) for n_i/N_0 from 0.1 [Fig. 4(a)], 0.15 [Fig. 4(b)], and 0.2 [Fig. 4(c)]. Though it is not clearly visible from real frequency curves, but from the growth rate curves, it is evident that the merging of the electron beam mode occurs with slow (red, dashed-dotted-dotted-dotted curve) and fast (blue, dashed curve) ion-acoustic modes. The $k\lambda_{de}$ range in which electron beam driven fast ion-acoustic mode (merging of mode 6 and 2) is unstable decreases slightly, whereas it increases for electron beam driven slow ion-acoustic modes. For instance, the $k\lambda_{de}$ ranges over which electron beam driven fast ion-acoustic mode is unstable for $n_i/N_0=0.10$, $n_i/N_0=0.15$, and $n_i/N_0=0.20$, respectively, are 0.62–2.92, 0.81–2.87, and 0.96–2.80.

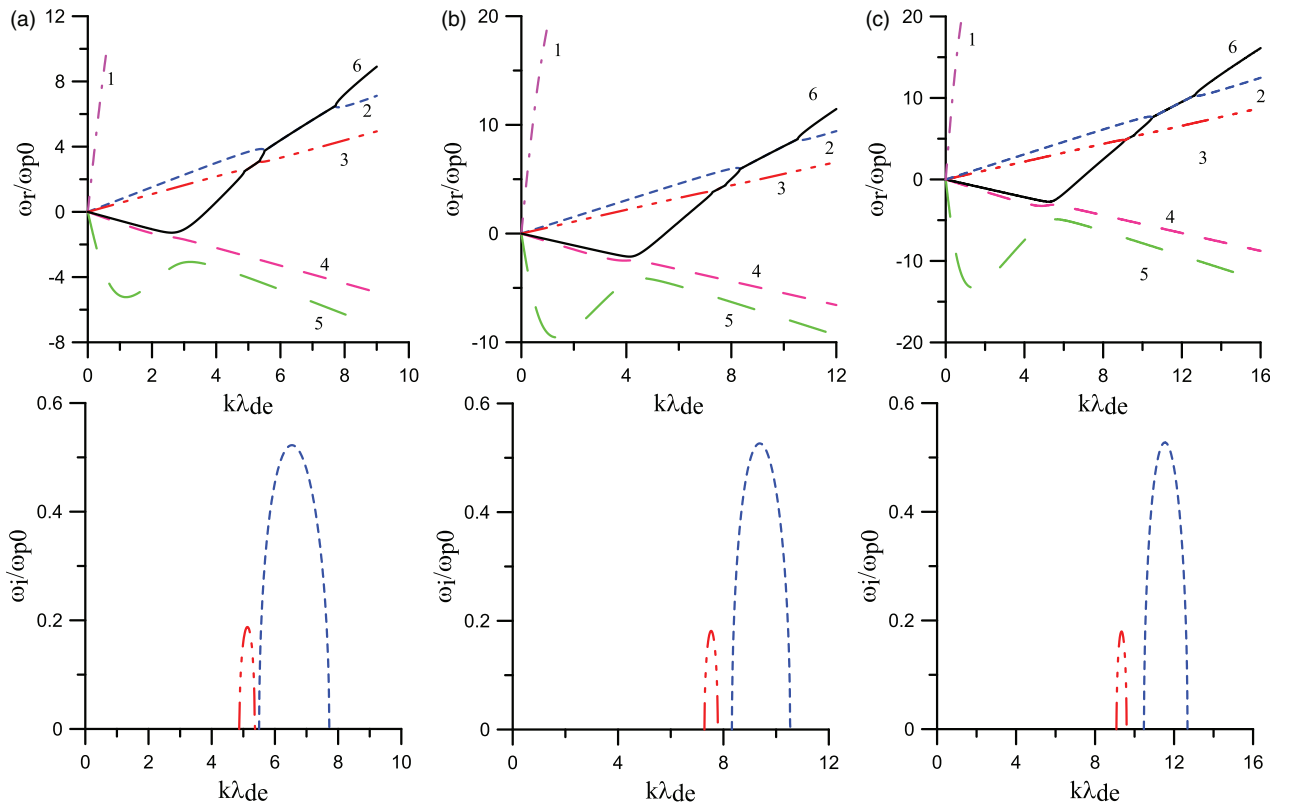


FIG. 3. Effect of n_b/N_0 variation on dispersion characteristics for $U_b/C_s=5$. The other fixed plasma parameters are the same as those in Fig. 1. (a) $n_b/N_0=0.1$, (b) $n_b/N_0=0.2$, (c) $n_b/N_0=0.3$.

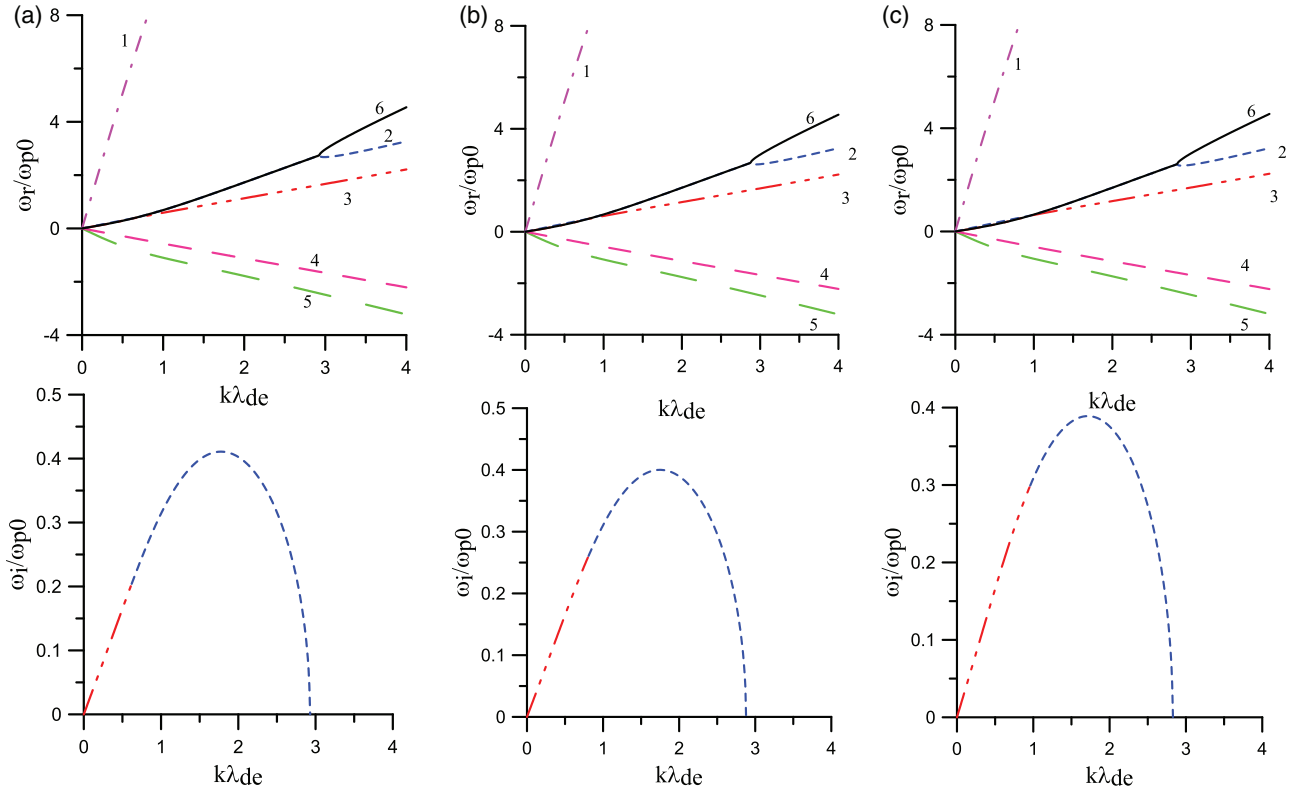


FIG. 4. Effect of n_i/N_0 variations on dispersion characteristics for $U_b/C_s = 5$. The other fixed plasma parameters are the same as those in Fig. 1. (a) $n_i/N_0 = 0.10$, (b) $n_i/N_0 = 0.15$, and (c) $n_i/N_0 = 0.20$.

D. Variation of electron beam temperature

In this section, we study the effect of the variation of temperature of electron beam on the growth of the electrostatic waves. The plasma parameters fixed for this variation are $n_i/N_0 = 0.05$, $n_b/N_0 = 0.01$, $\kappa = 6$, $T_p/T_e = 0.2$, $T_i/T_e = 0.4$, and $U_b/C_s = 5$. One of the most prominent features of this variation is the behavior of mode 6. In Fig. 5(a), the electron beam driven fast ion-acoustic mode becomes unstable in the range $k\lambda_{de} \approx 0-2.15$ for $T_b/T_e = 0.002$. The electron beam driven slow ion-acoustic mode along with fast ion-acoustic mode starts to appear as the electron beam temperature is increased further and slow and fast ion-acoustic modes are clearly distinguishable at $T_b/T_e = 0.0032$ [Fig. 5(b)]. In Fig. 5(b), the electron beam driven slow ion-acoustic mode is unstable in the range, $k\lambda_{de} \approx 1.5-2.5$, whereas for a higher range of $k\lambda_{de} \approx 4.3-13.9$ the fast ion-acoustic mode is unstable. When the value of T_b/T_e is further increased, the growth rate of the electron beam driven fast ion-acoustic mode becomes less than that of the electron beam driven slow ion-acoustic mode (not shown here). It is interesting to note that the electron beam driven fast ion-acoustic mode ceases to exist when the value of T_b/T_e reaches 0.00324. When T_b/T_e is increased to 0.0035, the electron beam driven slow ion-acoustic mode is the only unstable mode for a large value of $k\lambda_{de} (\approx 4.6-6.4)$. The electron beam driven slow ion-acoustic mode also disappears at $T_b/T_e = 0.004$. Overall, growth rates of both the modes, i.e., fast and slow ion-acoustic modes, decrease substantially with the increase in the T_b/T_e values.

E. Effect of temperature of ions

The effect of variation of temperature of ions is displayed in Fig. 6. For $T_i/T_e = 0.2$, the electron beam driven fast ion-acoustic mode is unstable in the range $k\lambda_{de} \approx 0-3$, whereas the slow ion-acoustic mode is stable. With a subsequent increase in T_i/T_e , the electron beam driven slow ion-acoustic mode become more unstable with a larger growth rate, whereas growth of the fast ion-acoustic mode decreases significantly. At $T_i/T_e = 1.4$, slow and fast ion-acoustic modes almost start to separate from each other and eventually separate as shown in Fig. 6(c) at $T_i/T_e = 1.8$. Initially, the electron beam driven fast ion-acoustic mode is excited for a large range of wavenumbers; however, as the ion temperature increases its range diminishes and also shifts to higher wavenumbers. The range of wavenumbers for which slow ion-acoustic mode is excited also diminishes with the increase in ion temperature. It is also observed (not shown here) that beyond $T_i/T_e = 2.3$, mode 6 interacts with mode 3 only, i.e., electron beam can drive only the slow ion-acoustic mode unstable.

F. Effect of temperature of protons

The effect of temperature of protons on the dispersion of the waves is plotted in Fig. 7. The ratio of temperature of protons to electrons, T_p/T_e , has been increased from 0.4 to 0.8. For $T_p/T_e = 0.4$, initially mode 6 merges with mode 3 with a maximum growth rate of electron beam driven slow ion-acoustic mode, $\omega_i/\omega_{p0} = 0.11$ and later on mode 6 merges with mode 2 and drives the fast ion-acoustic mode

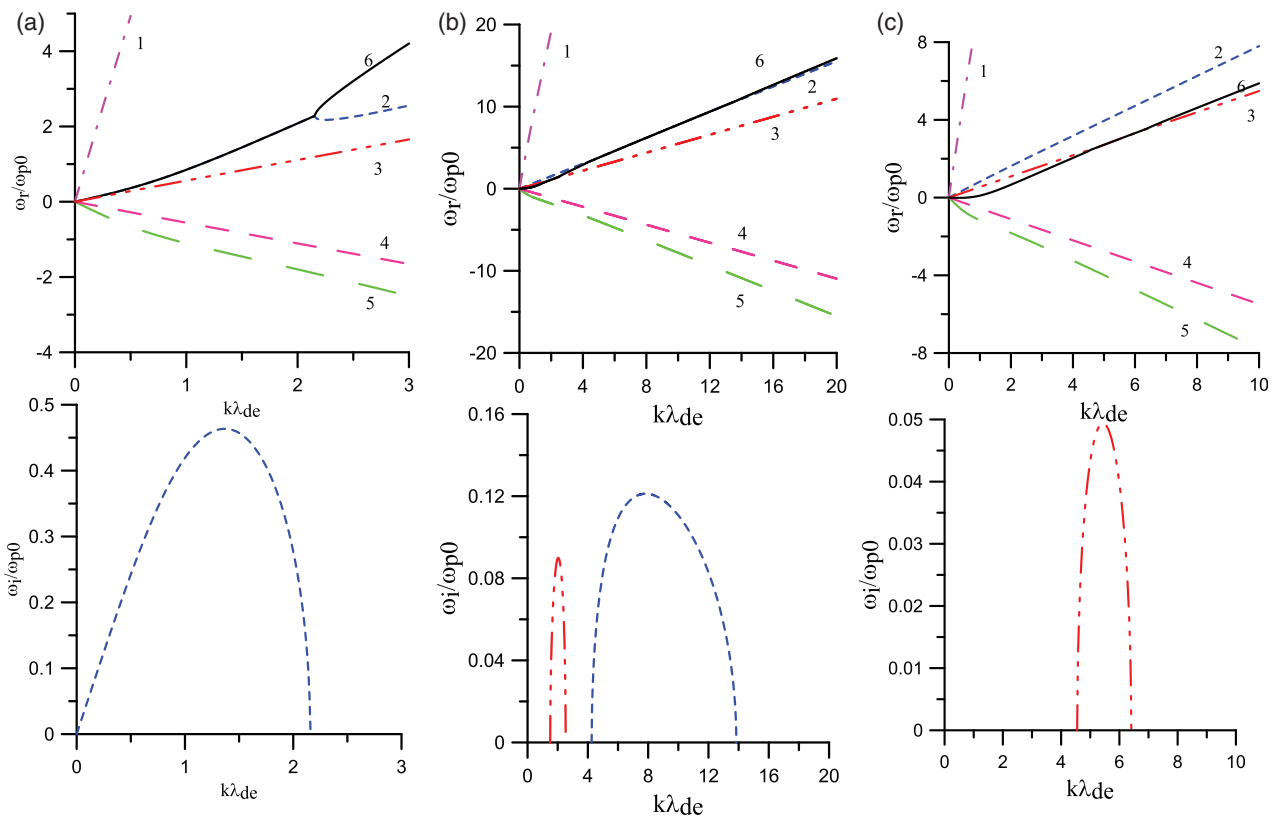


FIG. 5. Effect of T_b/T_e variations on characteristics of the waves for $U_b/C_s = 5$. The other fixed plasma parameters are the same as those in Fig. 1. (a) $T_b/T_e = 0.002$, (b) $T_b/T_e = 0.0032$, and (c) $T_b/T_e = 0.0035$.

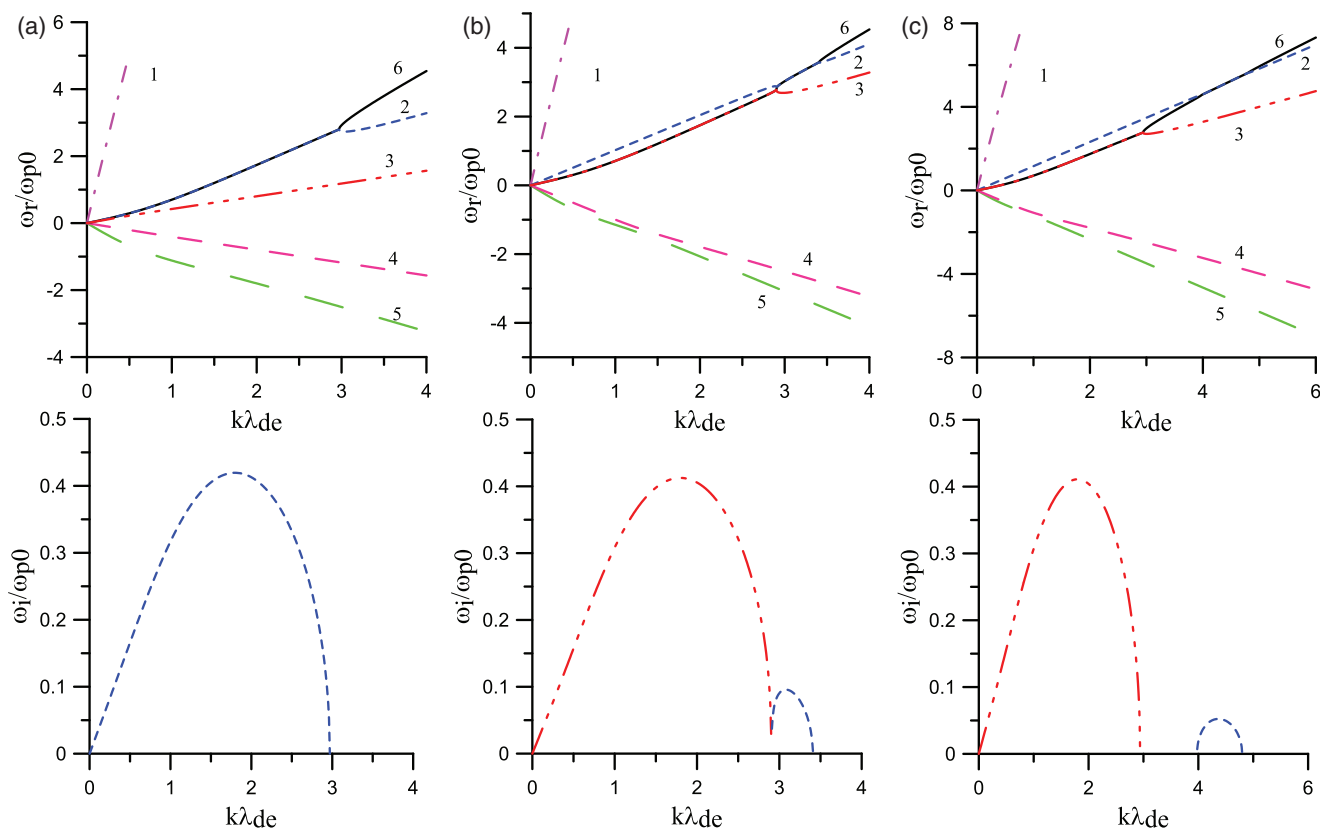


FIG. 6. Effect of T_i/T_e variations on characteristics of the waves for $U_b/C_s = 5$. The other fixed plasma parameters are the same as those in Fig. 1. (a) $T_i/T_e = 0.2$, (b) $T_i/T_e = 1.4$, and (c) $T_i/T_e = 1.8$.

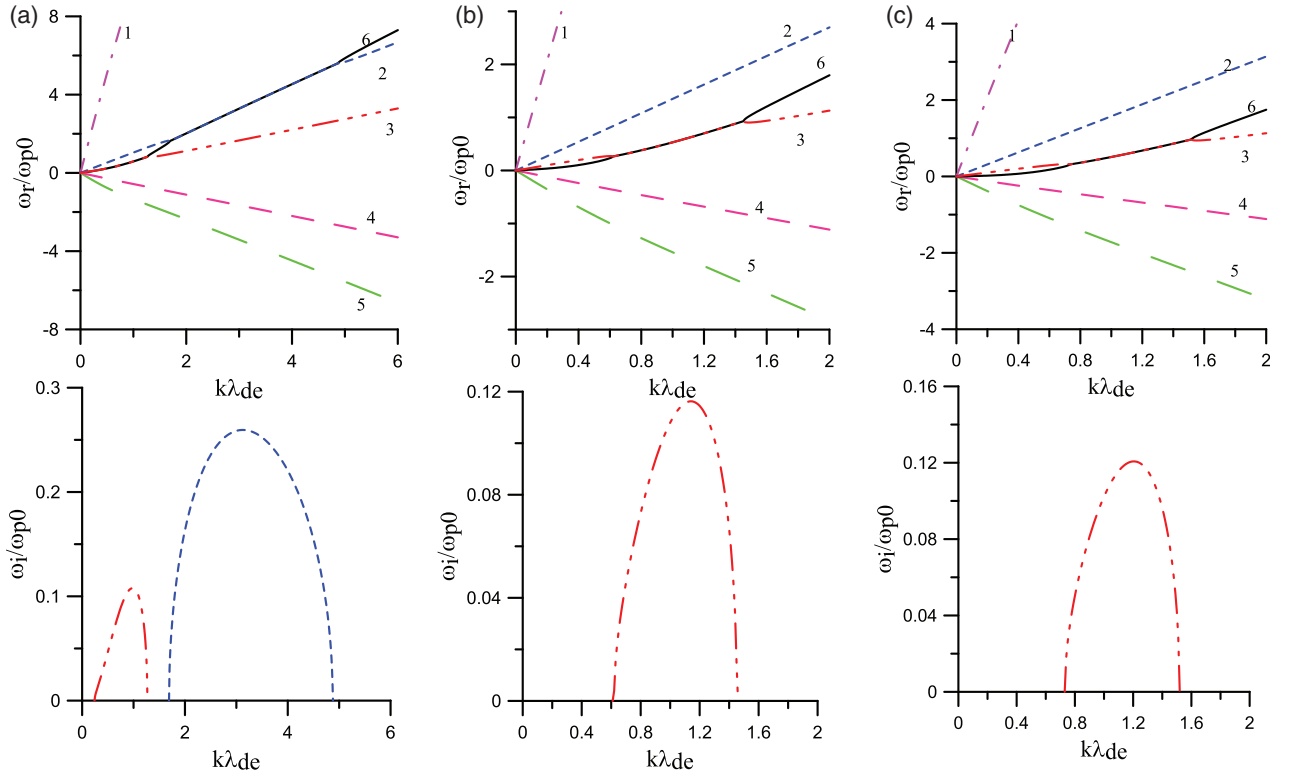


FIG. 7. Effect of T_p/T_e variations on characteristics of the waves for $U_b/C_s = 5$. The other fixed plasma parameters are the same as those in Fig. 1. (a) $T_p/T_e = 0.4$, (b) $T_p/T_e = 0.6$, and (c) $T_p/T_e = 0.8$.

unstable with a maximum growth rate, $\omega_i/\omega_{p0} = 0.26$. With a subsequent increase in T_p/T_e up to 0.553, both slow and fast ion-acoustic modes are unstable with the growth rate of the electron beam driven fast ion-acoustic mode becoming lesser than that of the slow ion-acoustic mode. Beyond $T_p/T_e > 0.553$, there is no interaction between modes 6 and 2, but mode 6 interacts with mode 3 and drives the slow ion-acoustic waves unstable. In general, as the temperature of the protons increases there is a slight increase in the maximum growth rate of electron beam driven slow ion-acoustic waves, whereas the growth rate of fast ion-acoustic mode decreases substantially and eventually the fast ion-acoustic mode vanishes.

IV. CONCLUSION

Recently, Tao *et al.*²⁰ have reported observation of electrostatic waves in the lunar wake during the first flyby of the Acceleration, Reconnection, Turbulence and Electrodynamics of the Moon's Interaction with the Sun (ARTEMIS) and performed 1-D Vlasov simulation on a four-component lunar wake plasma concluding that the observed electrostatic waves, in the frequency range $(0.1-0.4)f_{pe}$ (WB2/WB3), were most likely the electron beam mode in the wave bursts WB2 and WB3, whereas wave burst WB1 has a low-frequency component which can reach as low as $0.01f_{pe}$. The frequency of the wave burst in WB1 is closer to ion plasma frequency; therefore, ion dynamics becomes important. In this paper, we have carried out a linear analysis of parallel propagating electrostatic waves in a four component magnetized plasma comprising fluid protons, fluid He^{++} , electron beam, and suprathermal

electrons following kappa distribution. This theoretical plasma model is relevant to the lunar wake plasma. It is found that as the electron beam velocity is increased, mode 6 gets affected the most and starts to merge with mode 3 (slow ion-acoustic mode) and mode 2 (fast ion-acoustic mode) to form an unstable region with finite wave growth. It is observed that merging of modes 6 and 3 occurs at a smaller value of wavenumbers as compared to the merging of modes 6 and 2. Actually, the merging denotes a complex double root, where phase velocities of the electron acoustic and slow (fast) ion-acoustic modes become the same. This interaction results in one mode growing (positive imaginary part, unstable) and the other as damped (equal negative imaginary part). Here, we have shown only the unstable electron beam driven slow and fast ion-acoustic modes. The increase in number density and temperature of electron beam has an adverse effect on the electron beam driven slow ion-acoustic mode. On the other-hand, the growth rate of the electron beam driven slow ion-acoustic mode increases with an increase in number density of ions and temperatures of ions and protons. In the case of the electron beam driven fast ion-acoustic mode, the growth rate increases with an increase in electron beam density and decreases with an increase in ion number density and temperatures of the electron beam, ions, and protons. We have carried out numerical computation for the typical case of Fig. 2(a) where mode 6 merges first with the slow mode and thereafter with the fast mode. The frequency corresponding to the maximum growth rate of the electron beam driven slow ion-acoustic mode is $\omega_r = 0.03\omega_{pe}$ and for the electron beam driven fast ion-acoustic mode it is $\omega_r = 0.2\omega_{pe}$. These frequency estimates agree very well with the observed low-frequency waves

$\omega \approx 0.01\omega_{pe}$ (WB1) and high frequency waves $\omega \approx 0.1-0.4\omega_{pe}$ (WB2/WB3) in the lunar wake by Tao *et al.*²⁰

ACKNOWLEDGMENTS

G.S.L. thanks the Indian National Science Academy (INSA) for the support under the INSA Honorary Scientist scheme.

- ¹N. F. Ness, *J. Geophys. Res.* **70**, 517–534, <https://doi.org/10.1029/JZ070i003p00517> (1965).
- ²F. C. Michel, *J. Geophys. Res.* **73**, 7277–7283, <https://doi.org/10.1029/JA073i023p07277> (1968).
- ³J. M. Bosqued, N. Lormant, H. Rème, C. d’Uston, R. P. Lin, K. A. Anderson, C. W. Carlson, R. E. Ergun, D. Larson, J. McFadden, M. P. McCarthy, G. K. Parks, T. R. Sanderson, and K. Wenzel, *Geophys. Res. Lett.* **23**, 1259–1262, <https://doi.org/10.1029/96GL00303> (1996).
- ⁴N. F. Ness, in *Solar-Terrestrial Physics/1970: Proceedings of the International Symposium on Solar-Terrestrial Physics Held in Leningrad, U.S.S.R. 12–19 May 1970*, edited by E. R. Dyer (Springer Netherlands, Dordrecht, 1972), pp. 347–393.
- ⁵C. J. Owen, R. P. Lepping, K. W. Ogilvie, J. A. Slavin, W. M. Farrell, and J. B. Byrnes, *Geophys. Res. Lett.* **23**, 1263–1266, <https://doi.org/10.1029/96GL01354> (1996).
- ⁶K. W. Ogilvie, J. T. Steinberg, R. J. Fitzenreiter, C. J. Owen, A. J. Lazarus, W. M. Farrell, and R. B. Torbert, *Geophys. Res. Lett.* **23**, 1255–1258, <https://doi.org/10.1029/96GL01069> (1996).
- ⁷W. M. Farrell, M. L. Kaiser, J. T. Steinberg, and S. D. Bale, *J. Geophys. Res.* **103**, 23653–23660, <https://doi.org/10.1029/97JA03717> (1998).
- ⁸P. C. Birch and S. C. Chapman, *Geophys. Res. Lett.* **28**, 219–222, <https://doi.org/10.1029/2000GL011958> (2001).
- ⁹L. Xie, L. Li, Y. Zhang, and D. L. De Zeeuw, *Sci. China Earth Sci.* **56**, 330–338 (2013).
- ¹⁰S. I. Popel, G. E. Morfill, P. K. Shukla, and H. Thomas, *J. Plasma Phys.* **79**, 1071–1074 (2013).
- ¹¹S. I. Popel, L. M. Zelenyi, and B. Atamaniuk, *Phys. Plasmas* **22**, 123701 (2015).
- ¹²S. I. Popel and T. I. Morozova, *Plasma Phys. Rep.* **43**, 566–575 (2017).
- ¹³P. J. Kellogg, K. Goetz, S. J. Monson, J.-L. Bougeret, R. Manning, and M. L. Kaiser, *Geophys. Res. Lett.* **23**, 1267–1270, <https://doi.org/10.1029/96GL00376> (1996).
- ¹⁴T. Nakagawa, Y. Takahashi, and M. Iizima, *Earth, Planets Space* **55**, 569–580 (2003).
- ¹⁵W. M. Farrell, R. J. Fitzenreiter, C. J. Owen, J. B. Byrnes, R. P. Lepping, K. W. Ogilvie, and F. Neubauer, *Geophys. Res. Lett.* **23**, 1271–1274, <https://doi.org/10.1029/96GL01355> (1996).
- ¹⁶S. D. Bale, C. J. Owen, J.-L. Bougeret, K. Goetz, P. J. Kellogg, R. P. Lepping, R. Manning, and S. J. Monson, *Geophys. Res. Lett.* **24**, 1427–1430, <https://doi.org/10.1029/97GL01193> (1997).
- ¹⁷P. C. Birch and S. C. Chapman, *Phys. Plasmas* **9**, 1785–1789 (2002).
- ¹⁸N. Borisov and U. Mall, *Phys. Lett. A* **265**, 369–376 (2000).
- ¹⁹P. Travnicek, P. Hellinger, D. Schriver, and S. D. Bale, *Geophys. Res. Lett.* **32**, L06102, <https://doi.org/10.1029/2004GL022243> (2005).
- ²⁰J. B. Tao, R. E. Ergun, D. L. Newman, J. S. Halekas, L. Andersson, V. Angelopoulos, J. W. Bonnell, J. P. McFadden, C. M. Cully, H.-U. Auster, K.-H. Glassmeier, D. E. Larson, W. Baumjohann, and M. V. Goldman, *J. Geophys. Res.* **117**, A03106, <https://doi.org/10.1029/2011JA017364> (2012).
- ²¹R. Rubia, S. V. Singh, and G. S. Lakhina, *J. Geophys. Res.* **122**, 9134–9147, <https://doi.org/10.1002/2017JA023972> (2017).
- ²²G. S. Lakhina, S. V. Singh, A. P. Kakad, F. Verheest, and R. Bharuthram, *Nonlinear Processes Geophys.* **15**, 903–913 (2008).
- ²³G. S. Lakhina, S. V. Singh, and A. P. Kakad, *Phys. Plasmas* **21**, 062311 (2014).
- ²⁴S. K. Maharaj, R. Bharuthram, S. V. Singh, and G. S. Lakhina, *Phys. Plasmas* **22**, 032313 (2015).
- ²⁵G. S. Lakhina and S. V. Singh, *Sol. Phys.* **290**, 3033–3049 (2015).
- ²⁶C. P. Olivier, S. K. Maharaj, and R. Bharuthram, *Phys. Plasmas* **22**, 082312 (2015).
- ²⁷R. Rubia, S. V. Singh, and G. S. Lakhina, *Phys. Plasmas* **23**, 062902 (2016).
- ²⁸R. Rubia, S. V. Singh, and G. S. Lakhina, *Phys. Plasmas* **25**, 032302 (2018).
- ²⁹D. Summers and R. M. Thorne, *Phys. Fluids B* **3**, 1835–1847 (1991).
- ³⁰S. Devanandhan, S. V. Singh, G. S. Lakhina, and R. Bharuthram, *Nonlinear Processes Geophys.* **18**, 627–634 (2011).
- ³¹S. Devanandhan, S. V. Singh, and G. S. Lakhina, *Phys. Scr.* **84**, 025507 (2011).
- ³²S. Devanandhan, S. V. Singh, G. S. Lakhina, and R. Bharuthram, *Commun. Nonlinear Sci. Numer. Simul.* **22**, 1322–1330 (2015).
- ³³A. Mangeney, C. Salem, C. Lacombe, J. L. Bougeret, C. Perche, R. Manning, P. J. Kellogg, K. Goetz, S. J. Monson, and J. M. Bosqued, *Ann. Geophys.* **17**, 307–320 (1999).